J. Fluid Mech. (2007), *vol.* 580, *pp.* 319–338.
doi:10.1017/S0022112007005435 Printed in the United Kingdom

Near-surface particle image velocimetry measurements in a transitionally rough-wall atmospheric boundary layer

SCOTT C. MORRIS[1], SCOTT. R. STOLPA[1], PAUL E. SLABOCH[1] AND JOSEPH C. KLEWICKI[2]

[1]Aerospace and Mechanical Engineering, University of Notre Dame, Notre Dame, IN 46556, USA
s.morris@nd.edu
[2]Mechanical Engineering, University of New Hampshire, Durham, NH 03824, USA

(Received 10 February 2006 and in revised form 12 December 2006)

The Reynolds number dependence of the structure and statistics of wall-layer turbulence remains an open topic of research. This issue is considered in the present work using two-component planar particle image velocimetry (PIV) measurements acquired at the Surface Layer Turbulence and Environmental Science Test (SLTEST) facility in western Utah. The Reynolds number ($\delta u_\tau/\nu$) was of the order 10^6. The surface was flat with an equivalent sand grain roughness $k^+ = 18$. The domain of the measurements was $500 < yu_\tau/\nu < 3000$ in viscous units, $0.00081 < y/\delta < 0.005$ in outer units, with a streamwise extent of $6000\nu/u_\tau$. The mean velocity was fitted by a logarithmic equation with a von Kármán constant of 0.41. The profile of $\overline{u'v'}$ indicated that the entire measurement domain was within a region of essentially constant stress, from which the wall shear velocity was estimated. The stochastic measurements discussed include mean and RMS profiles as well as two-point velocity correlations. Examination of the instantaneous vector maps indicated that approximately 60 % of the realizations could be characterized as having a nearly uniform velocity. The remaining 40 % of the images indicated two regions of nearly uniform momentum separated by a thin region of high shear. This shear layer was typically found to be inclined to the mean flow, with an average positive angle of 14.9°.

1. Introduction

The phenomenology of wall layer turbulence has been studied for over a century, and continues to be a topic of active research. The importance of turbulent boundary layers in many engineering applications provides motivation to understand this flow in detail. An unresolved issue of importance in the study of turbulent boundary layers is that of Reynolds number dependence. Because many applications operate at large Reynolds numbers, it is important to assess how quantities of interest vary as the Reynolds number is increased. Detailed experimental data are, however, limited given the difficulty of obtaining adequate spatial resolution in high-Reynolds-number laboratory flows. For example, reducing the kinematic viscosity of the working fluid (e.g. McKeon *et al.* 2004 and DeGraaff & Eaton 2000) is an effective method to generate a high Reynolds number, but produces a relatively small viscous length, ν/u_τ, (where $u_\tau = \sqrt{\tau_{wall}/\rho}$ is the friction velocity, τ_{wall} is the surface shear stress, ρ is the density, and ν is the kinematic viscosity) which makes detailed, multi-point spatial

measurements difficult. High-Reynolds-number measurements with adequate spatial resolution are typically limited by the available space in most laboratories.

A strategy for accessing the structure of wall-bounded flows under very high-Reynolds-number conditions is to acquire data in the atmospheric boundary layer. The Surface Layer Turbulence and Environmental Science Test (SLTEST) site was recently developed by Klewicki and coworkers. This facility provides nearly ideal conditions with flat terrain and predictable winds. A significant body of research has come from this facility in the last decade. See, for example, Klewicki *et al.* (1995), Metzger *et al.* (2001), Metzger & Klewicki (2001), Morris & Foss (2003, 2005), Hommema & Adrian (2003), Marusic & Kunkel (2003), Priyadarshana & Klewicki (2004), Kunkel & Marusic (2006), and McNaughton, Clement & Moncrieff (2006), and references therein.

The goal of the present research was to acquire particle image velocimetry (PIV) measurements at the SLTEST site in order to provide new information about wall turbulence at very high Reynolds number. PIV is advantageous because planar realizations of the flow field including both u and v components are obtained. This allows standard stochastic quantities such as mean velocity, Reynolds stress profiles, and two-point spatial correlations to be computed easily. The data also provided visualization of the instantaneous structure of the flow fields in order to better understand the organized motions of the wall-layer flow at high Reynolds number.

It is instructive to consider the length and time scales of a high-Reynolds-number boundary layer compared to more familiar laboratory flows. The atmospheric surface layer thickness at the SLTEST site is typically of order 100 m. The ratio of the outer length scale to the viscous length is given by the Reynolds number defined as $\delta^+ = \delta u_\tau/\nu$ where δ is the surface layer thickness. In previous SLTEST measurements Metzger *et al.* (2001) and Priyadarshana & Klewicki (2004) found $\delta \approx 100$ m, in agreement with the estimate given by Stull (1988) for atmospheric flow over smooth terrain. The corresponding value for the present data set was $\delta^+ \approx 600\,000$.

The domain of the present experiments was different from laboratory measurements in terms of the inner (viscous) and outer scaling. Specifically, the PIV field of view was $0.08 < y < 0.48$ m, which corresponded to $500 < y^+ < 3000$, where $y^+ = yu_\tau/\nu$, or $0.00081 < y/\delta < 0.005$. Even in the highest-Reynolds-number laboratory flows, $y^+ = O(10^3)$ is outside the log-linear region of the mean velocity profile. For example, DeGraaff & Eaton (2000) show a deviation from the standard law of the wall at $y^+ = 2800$ for $Re_\theta \approx 31\,000$, where θ is the momentum thickness of the boundary layer. Similarly, the range of y/δ obtained in the present work is well within the viscous sublayer in most laboratory boundary layers. In summary, the measurement domain considered here in terms of both inner and outer scaling only exists in very high-Reynolds-number boundary layers.

Also of interest is the roughness length of the surface compared to the inner and outer scales. Visual observations and data presented below indicated a surface roughness height of about 3 mm. In viscous units the equivalent sand grain roughness was determined to be $k^+ \approx 18$, or equivalently $\delta/k = O(10^4)$. In other words, the surface is extremely smooth compared to the boundary layer thickness, yet transitionally rough in terms of the viscous units.

This discussion of the Reynolds number and length scales involved sets the context for the research questions addressed by the present work. First, how do the statistics such as mean velocity, RMS values, Reynolds stresses, and two-point correlation functions compare to a lower-Reynolds-number boundary layer? This question is addressed in detail in § 3. A second question, addressed in § 4, is related to the

instantaneous structure of the turbulence. Specifically, how do the turbulent motions that contribute to the statistics compare with the dynamic structure observed at low Reynolds number? The data reported will include example realizations of the flow to convey the general appearance of the wall-layer structure.

2. Experimental measurements

2.1. *Description of the SLTEST site*

The measurement results presented in this paper were acquired at the SLTEST site. The facility is located at the southern end of the Great Salt Lake Desert (113°26.5′W, 40°8.1′N) on the US Army's Dugway Proving Ground in western Utah, USA. The terrain around the test site is extremely smooth, with variations in elevation less than 1 m over the first 13 km north of the test site, and generally free from obstruction for about 100 km upwind of the measurement station. A steady North wind is often present during early summer months which allows data collection under nearly stationary conditions.

Data were acquired during a two week period in June 2003, and a one week period in June 2004. The data that were collected from 20:25 until 20:55 (CDST) on 19 June 2004 will be described in detail herein. Although all of the data from the various experimental trials are qualitatively (and quantitatively) similar, the 19 June 2004 data provided the best combination of equipment function and environmental conditions as described below. The wind direction was NNE, with a speed of roughly 2.1 m s^{-1} at 0.5 m from the surface. A total of 708 realizations were acquired.

The surface conditions at the test site can vary from one day to the next depending on local weather patterns. The surface material is generally solid and free from loose debris and dust. A moderate rainfall occurred on the evening of 17 June 2004 which smoothed the surface to a nominal roughness of 2–3 mm. The moisture also made the surface resistant to footprints which can be created as the research group moves about the setup.

2.2. *Thermal surface boundary conditions*

An important consideration for atmospheric measurements is the thermal stability of the surface layer. The data were acquired during the evening hours, and the surface layer was in a transition from unstable to stable stratification. The thermal stability can be explained in terms of the approximate turbulent kinetic energy budget (Kaimal & Finnigan 1994):

$$\frac{\mathrm{D}\bar{e}}{\mathrm{D}t} = 0 = \underset{\mathrm{I}}{-(\overline{u'v'})\frac{\partial \bar{u}}{\partial y}} + \underset{\mathrm{II}}{\frac{g}{\theta}(\overline{v'\theta'})} + \underset{\mathrm{III}}{\frac{1}{\rho}\frac{\partial}{\partial y}(\overline{v'p'})} - \underset{\mathrm{IV}}{\frac{\partial}{\partial y}(\overline{e'v'})} - \underset{\mathrm{V}}{\varepsilon} \tag{1}$$

which assumes negligible transport due to the mean flow or viscous effects. Note that in the present notation y is the surface-normal direction, whereas z is generally used in the atmospheric boundary layer literature. Term I is the shear production that results from the mean shear and Reynolds stress. Term II can be a source or a sink of turbulent fluctuations depending on the sign of $\overline{v'\theta'}$, where θ' is the potential temperature fluctuation. Terms III, IV, and V represent the pressure diffusion, turbulent transport, and dissipation, respectively.

The balance of the terms can be clarified by first multiplying equation (1) by the log-layer dissipation estimate, $\kappa y/u_\tau^3$, where κ is the von Kármán constant. The first

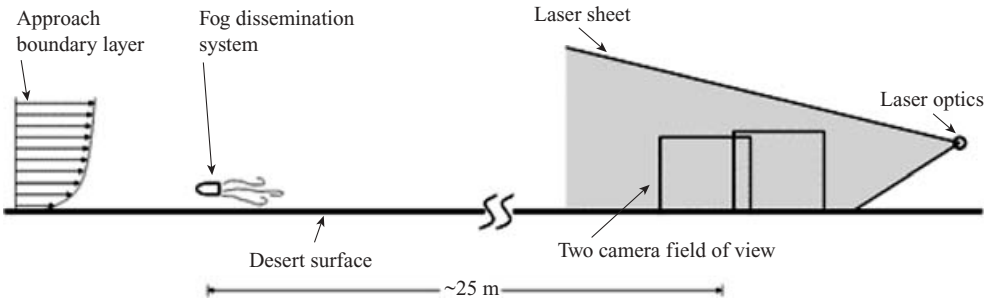

FIGURE 1. Schematic of experimental set-up.

term is simplified by the assumption that the mean velocity nominally follows a logarithmic profile with logarithmic slope equal to $1/\kappa$, and that the Reynolds stress is a constant value: $\overline{u'v'} \approx u_\tau^2$. These assumptions are supported by the data discussed in § 3. Term I is therefore unity over the measurement domain. Term II becomes the Monin–Obukhov stability parameter:

$$\frac{y}{L} \equiv -\frac{g}{\theta}(\overline{v'\theta'})\frac{\kappa y}{u_\tau^3}. \tag{2}$$

The quantity y/L is recognized as an appropriate stability parameter relevant to characterizing the effects of buoyancy. Note that the ratio of term II to term I is defined as the flux Richardson number, and is identical to y/L in the limit of the assumptions given for term I.

Data from three sonic anemometers located at heights of 1.26 m, 2.9 m, and 3.9 m were used to obtain time series records of the turbulent heat flux. The magnitude of L was found to vary by less than a few percent from the three elevations, and was nearly stationary for one hour prior to, and two hours after, the acquisition of the PIV data. An average magnitude of $|L| \approx 2$ m was found during the 25 minutes of PIV data. Assuming a constant heat flux ($L =$ constant), the stability parameter varies linearly with wall normal distance so that $0.04 < |y/L| < 0.25$. That is, the shear production of turbulence was roughly 25 times larger than the buoyancy term in the lower region of the measurements. In the upper region of the measurement plane, shear production was approximately four times larger than buoyancy production. Although term I is the dominant production term throughout the measurement region, a value of $y/L \approx -0.25$ indicates that buoyancy can change the overall balance of equation (1). This suggests that care should be taken when comparing the present measurement results to those of neutral boundary layers, particularly at the measurement locations furthest from the surface. Additional commentary will be provided in this regard throughout the description of the measurement results.

2.3. *Particle image velocimetry set-up*

The data presented in this paper were acquired using a standard LaVision PIV system. A schematic of the set-up is shown in figure 1. The laser was a dual 120 mJ Nd-Yag with a light arm to house the optics. Two cameras with 2048 by 2048 pixel resolution were placed side-by-side, at a distance of 2 m from the laser sheet. This provided a field of view of nominally $0.08 < y < 0.5$ m in the wall-normal direction, and 1.0 m in the streamwise direction. At locations closer to the wall ($y < 0.08$ m) the data were contaminated by the reflection of the laser from the ground. Bandpass optical filters

and mechanical shutters were used to limit the ambient light entering the cameras. The time delay between the image pairs was 1.0 ms for all of the data presented.

The image processing computer, laser, and cameras were all placed on a mobile cart that allowed the equipment to be protected from excessive daytime solar radiation, blowing sand (during storms), and rain. The data cart was equipped with two cantilevered I-beams to hold the cameras and laser optics in a fixed orientation.

The boundary layer was seeded using a fog dissemination device. The design intent was to seed the boundary layer with a minimal disturbance to the flow field. A small blower was used to pressurize a box which contained a Rosco 2600 fog generation machine. A flexible tube with 7.6 cm diameter and 7.5 m length connected the box to a hollow D-shaped fog release system that is shown schematically in figure 1. The box and fog machine were placed as far from the measurement and seeding release locations as possible. The D-shaped release device was 2.5 cm by 8 cm in cross-section, and 2 m in (spanwise) length, positioned 15 cm from the surface. The seeded air delivered from the pressurized box through the tube was distributed evenly through the 2 m span of the release tube. The fluid was ejected over the downstream portion of the D-shape at approximately the same velocity as the approach flow in order to minimize the jet/wake created by the seeding system. The device was placed roughly 25 m upstream of the measurement location. The dissemination of fog was wide enough to maintain seeding in the measurement volume during events of large spanwise turbulent motion.

At two instances during the data acquisition the mean wind shifted about 5° to the east, at which time the seeding system was moved, and the data cart was rotated such that the laser was pointed in the upwind direction. The effect of off-alignment of the laser with the mean flow direction is a 'cosine' type of error. Since the images were all acquired with less than 5° of variability, this constitutes less than 1 % error in the measured streamwise velocities.

The final vector processing was calculated using a multi-pass method with a final resolution that used 32 by 32 pixel interrogation windows with 50 % overlap. The resulting spatial resolution was 4 mm, or 24 viscous units. Vector validation was used including range and correlation peak methods. The average validation rate was 95 % for the 708 realizations acquired. The evaluation of statistical quantities presented in the following sections used both time and horizontal averages using only the validated vectors. This resulted in well-converged statistics (i.e. less than one percent variability) for both the time-averaged velocities and the second-order statistics.

2.4. *Data detrending*

An important issue when considering atmospheric data is the non-stationarity of the flow. Although the winds were extremely steady by atmospheric standards, comparison of the results to laboratory conditions requires a careful examination of the long-time behaviour of the velocity trends. A number of general methods exist in the literature for data detrending, e.g. Kaimal & Finnigan (1994). The main feature of these methods is to make a distinction between long-time transients and the unsteadiness of the turbulent motions of interest. This distinction is typically made in terms of the time scales of the unsteadiness. It is noted that the process of detrending necessarily involves a degree of subjectivity, particularly since the largest scales of turbulent boundary layer flow are known to be more than 10δ in the streamwise direction (Hutchins & Marusic 2006). The effect of high-pass filtering will typically reduce the magnitude of second-order statistics, and will reduce the spatial extent of two-point correlations.

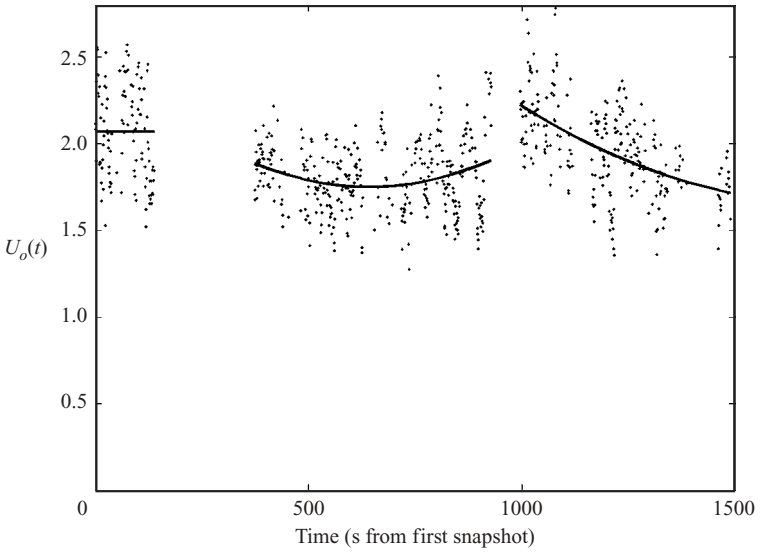

FIGURE 2. Time series of $U_o(t_i)$. Start time 22:24 (CDST).

The PIV data were detrended as follows. First, a spatial average of the flow domain was calculated for each instantaneous realization. Specifically,

$$U_o(t_i) = \frac{1}{L_x L_y} \int_0^{L_y} \int_0^{L_x} u(x, y, t_i)\, \mathrm{d}x\, \mathrm{d}y, \tag{3}$$

where L_x and L_y represent the streamwise and wall-normal extent of the full field of view. The results of this calculation for the time period of the data considered here are shown in figure 2. These data show significant frame to frame variation that results from the convecting turbulence. Additionally, the data reveal a slow variation in the spatial mean velocity over the measurement period. The surface-layer thickness can be estimated to be of order 100 m, and the observed mean velocity was $2\,\mathrm{m\,s^{-1}}$ or greater. Thus, the turbulent time scale associated with one boundary layer thickness should be about 50 s or less. The present strategy assumed that non-zero correlations over time scales longer than, say, 5 minutes are a result of larger-scale transients, and are not related to the mechanically generated turbulence due to the no-slip wall condition.

The $U_o(t_i)$ data were curve fitted using a third-order polynomial applied to three separate segments of the time series as shown in figure 2. Three separate fitting functions were chosen because small (5°) changes in wind direction occurred twice during the measurement period, corresponding to the two gaps in the time series shown in figure 2. The PIV equipment was realigned into the streamwise direction as described above, and data acquisition resumed. All of the velocities measured were then detrended as

$$u_i^*(x, y, t) = \frac{u_i(x, y, t)}{[U_o(t_i)]_{fit}} \overline{U}_o \tag{4}$$

where $\overline{U}_o$ represents the time-averaged value of $\overline{U}_o(t_i)$ over the entire measurement period. This calculation provided an effective high-pass filter that removed the drifting mean flow speed. The calculations described in the remainder of the paper were computed using the detrended values.

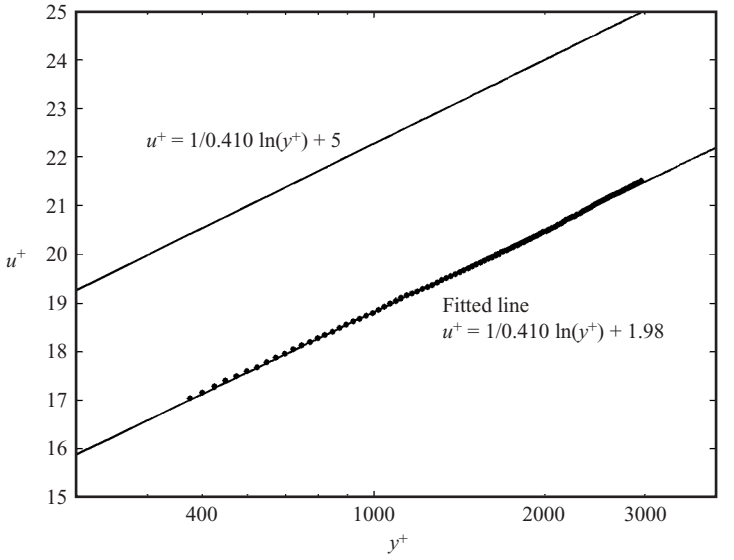

FIGURE 3. Mean velocity profile.

3. Boundary layer profile statistics

3.1. *Streamwise mean velocity*

The mean velocity profile is perhaps the best understood feature of wall-bounded flows. The form of the mean velocity is most often given by

$$u^+ = \frac{1}{\kappa}\log(y^+) + B - \Delta U^+ \tag{5}$$

where $\kappa \approx 0.41$ is the von Kármán constant, $B \approx 5$ is the smooth-wall offset, and ΔU^+ is a shift in the mean profile due to surface roughness. The mean profile derived from the present measurements is shown in figure 3. The value of $u_\tau = 0.094\,\mathrm{m\,s^{-1}}$ and its uncertainty ($\pm 5\,\%$) were estimated from the Reynolds stress data described below. The profile is clearly linear in the semilog plot, and offset from the smooth-wall condition by $\Delta U^+ = 3.02$. This suggests a transitionally rough surface with a roughness length scale of $k^+ \approx 18$ as determined from the data compiled by Jimenez (2004). Dimensionally, this corresponds to a roughness height of approximately 3 mm, which is consistent with the observed roughness of the ground surface.

The best-fit slope of the mean profile indicates a value of $\kappa = 0.410 \pm 0.02$. Given the precision by which κ can be determined in highly controlled laboratory studies, it is not rational to expect that the atmospheric measurements can contribute to questions relating to the true value of κ. However, it is interesting that the present estimate shows good correspondence with the value often accepted as the best estimate of κ from laboratory experiments (see e.g. DeGraaff & Eaton 2000). The value measured here confirms, at a minimum, that the various uncontrolled atmospheric effects (thermal stability, flow stationarity, surface roughness, etc.) have at most a modest effect on the mean velocity profile, and that the surface layer produces a Kármán constant that is within the uncertainty given in the present literature. Furthermore, this result reinforces the notion that the Kármán constant is at most a weak function of the Reynolds number.

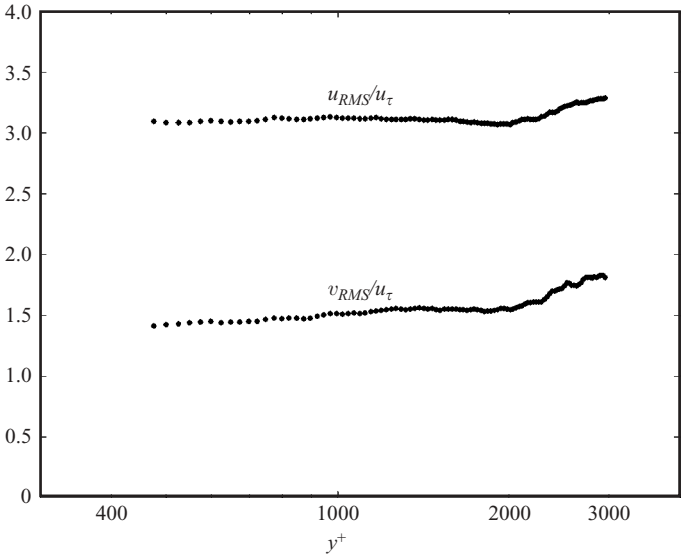

FIGURE 4. RMS profiles.

3.2. *Intensities and Reynolds stresses*

The root-mean-square values of the fluctuating velocity components are known to exhibit Reynolds number dependence. These statistics are difficult to obtain in many high-Reynolds-number flows given the limitations of probe resolution in small-scale laboratory environments. Data are particularly rare for the wall-normal component of velocity.

A thorough review of the available data has been provided by Gad-el-Hak & Bandyopadhyay (1994). More recently, DeGraaff & Eaton (2000) obtained both u and v component statistics for Reynolds numbers up to $Re_\theta = 31\,000$. The values of u_{rms} are known to exhibit significant Reynolds number dependence in the logarithmic region. For example, DeGraaff & Eaton (2000) show increasing RMS values (in wall units) as the Reynolds number is increased. Additionally, the highest-Reynolds-number measurements indicate that the values are roughly constant with respect to wall distance throughout much of the logarithmic region. This is in strong agreement with the results of Gad-el-Hak & Bandyopadhyay (1994), Marusic, Uddin & Perry (1997), Fernholz *et al.* (1995), Priyadarshana & Klewicki (2004), and others.

The u_{rms} values from the present measurements are shown in figure 4. These data show a roughly constant magnitude of $u_{rms}/u_\tau \approx 3.1$ over the range measured. It is of interest to compare this value with the similarity formulation proposed by Marusic *et al.* (1997). This model was previously shown to correctly predict u_{rms} in the logarithmic layer, which increases linearly as a function of $\log(\delta^+)$. Their model predicts a value of $u_{rms}/u_\tau = 3.1$ for $\delta^+ = 600\,000$ at $y^+ = 500$, in agrement with the estimate made earlier based on $\delta \approx 100$ m. Similar results including SLTEST data can be found in Marusic & Kunkel (2003), and Kunkel & Marusic (2006).

Figure 4 also shows an increase of about 25 % in the RMS values at large y^+. Previous measurements (both hot-wire and PIV) at the SLTEST site indicate similar phenomena, but not consistently. For example, PIV measurements on 2 June 2003 indicated a decrease in u_{rms} with y^+ under slightly stable conditions (Stolpa 2004). The cause of the increase in the present data is believed to be the effect of term II

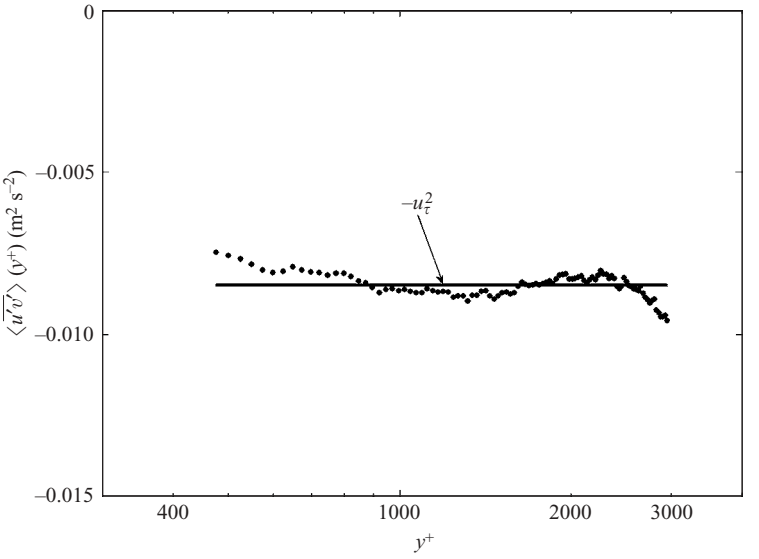

FIGURE 5. Reynolds stress profile.

in the kinetic energy budget. That is, the magnitude of y/L is large enough at the outer portion of the PIV domain that the buoyancy production of turbulence is no longer negligible. This is consistent with results shown in Panofsky & Dutton (1983) where v_{rms} values are presented as a function of y/L (their figure 7.1), which shows a moderate influence of the stability on RMS statistics for $y/L < -0.1$.

The RMS of the wall-normal component of velocity is also shown in figure 4. These values, like u_{rms}, are essentially flat over the region of the measurements, with a slight increase in magnitude at larger y^+. It is of interest to note that the ratio $u_{rms}/v_{rms} \approx 2$ obtained in the present measurements agrees well with the lower-Reynolds-number results of DeGraaff & Eaton (2000).

The Reynolds stress values are shown in figure 5. Like the RMS statistics, the observed values are roughly constant over the range of locations measured, as expected at this Reynolds number. There is, however, a local minimum in value located at $y^+ \approx 1400$, and a sharp decrease at higher y^+ magnitudes. This latter feature is similar to the observations regarding the component RMS levels, and could be related to thermal stability. The existence of a local minimum in the Reynolds stress could be a natural result of the mechanically (shear) generated turbulence. Sreenivasan (1989) correlated experimental data from lower Reynolds numbers and determined that this local minimum is related to the outer length scale by $y^+_{peak} \approx 2\sqrt{\delta^+}$. The observed y^+ peak corresponds to $\delta^+ = 490\,000$, in good agreement with initial estimates of the surface-layer thickness, as well as the estimate of $\delta^+ = 600\,000$ based on Marusic's theory from the measured values of u_{rms}/u_τ.

The Reynolds stress measurements can be normalized to a correlation coefficient: $\overline{u'v'}/(u_{rms}v_{rms})$. Given that the value of each of these variables is approximately constant, the value for this coefficient can be estimated to be 0.21 for the present measurement domain. Priyadarshana & Klewicki (2004, figure 3) compiled estimates of the Reynolds stress coefficient from a large number of studies, and showed a roughly linear decrease in the magnitude proportional to $\log(Re_\theta)$. The value obtained here is

in very good agreement with their results. Specifically, their curve fit predicts a value of 0.22 at $\delta^+ = Re_\theta \approx 5 \times 10^5$.

The friction velocity was estimated by the stress balance:

$$\overline{u'v'} = u_\tau^2. \tag{6}$$

Laboratory results with independent wall shear stress measurements agree that equation (6) is accurate in the limit of high Reynolds number (e.g. DeGraaff & Eaton 2000 and Fernholz *et al.* 1995). Moreover, previous results from the SLTEST site using a 2.4 m diameter drag plate show good agreement with the Reynolds-stress-based estimate. The data shown in figure 5 were averaged (spatially) in order to estimate $u_\tau = 0.094\,\mathrm{m\,s^{-1}}$. Simultaneous measurements from nearby sonic anemometers at wall distances of 1.26 m, 2.90 m, and 3.90 m all agreed with the value obtained from the averaged PIV data to within 5 %. This result adds confidence to the estimate of u_τ, and also confirms that an approximately constant stress layer exists over a region near the surface. This also suggests that the anomalous values of the Reynolds stress at the larger y^+ values noted in figure 5 may be localized, although a definitive explanation for this cannot be offered. The overall uncertainty in u_τ is estimated to be approximately 5 %. This is based on the variability of the Reynolds stress shown in figure 5, the agreement with the sonic anemometers, and previous experience relating the Reynolds stress to drag-plate data at the SLTEST site. Furthermore, the determination of the von Kármán constant described in § 3.1 is highly dependent on the value of u_τ used. The consistency of κ with laboratory results adds further confidence that equation (6) provides a reasonable estimate for u_τ.

3.3. *Two-point correlation functions*

The two-point velocity correlation is defined as

$$R_{u_i u_j}(\Delta x, y, y_{ref}) = \frac{\langle u_i(0, y_{ref}) u_j(\Delta x, y)\rangle}{\sigma_{u_i}(y_{ref})\sigma_{u_j}(y)} \tag{7}$$

where σ is the standard deviation of the velocity components, y_{ref} is a fixed wall-normal location, and the brackets denote the time average. A significant body of information exists regarding the two-point correlations in wall-bounded flows. For example, Metzger & Klewicki (2001) present spatial correlations using a time delay and Taylor's hypothesis in the very near-surface region ($y^+ < 20$) at the SLTEST site. Measurements of the space–time correlation in the outer region of laboratory boundary layers have been made by, for example, Kovasznay, Kibens & Blackwelder (1970). An important attribute of PIV is the availability of full planar information. The two velocity components recovered allowed the calculation of four of the two-point correlations from the u, v measurements: R_{uu}, R_{vv}, R_{uv}, and R_{vu}. These data are shown in figures 6 and 7 for fixed reference positions $y^+ = 524$, 943, 1906, and 2893.

A number of important features can be observed in the R_{uu} data, especially when compared to previous laboratory results. First, the contours of constant correlation magnitude are roughly elliptical in shape with the major axis tilted at an angle to the streamwise direction. The correlation length in the streamwise direction is large. For example, figure 6 shows that with a fixed point at $y^+ = 524$ the $R_{uu} = 0.5$ contour extends to $|\Delta x^+| > 5000$. Similar features have been observed in a number of previous studies at much lower Reynolds number. For example, the 'tilt' in the contours of constant correlation magnitude were reported in the space–time correlations of Kavosznay *et al.* (1970), and later observed without the use of Taylor's hypothesis using PIV measurements in Ganapathisubramani *et al.* (2005), Christensen & Wu

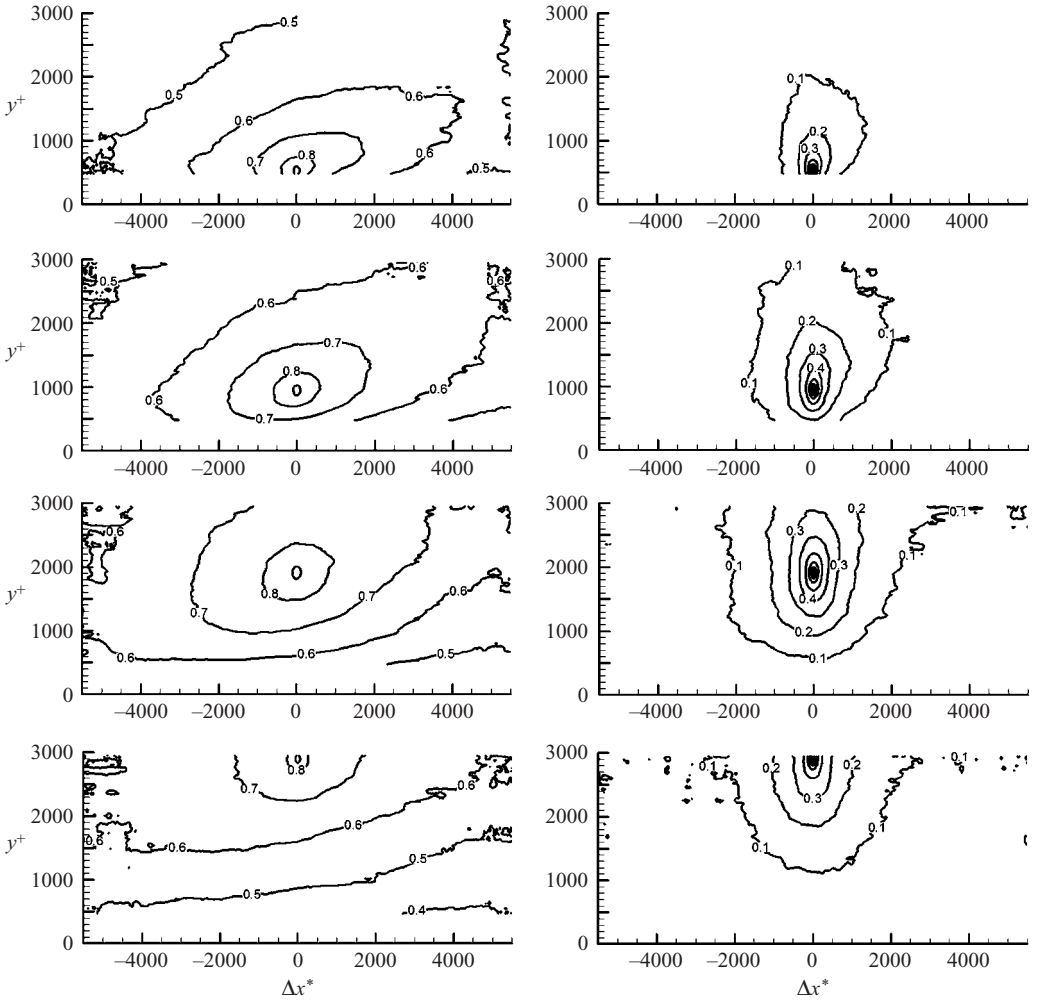

FIGURE 6. Two-point correlation functions R_{uu} (left) and R_{vv} (right). Fixed-point values for the four rows of figures are $y^+_{ref} = 524$, 943, 1906, and 2893, respectively.

(2005), and Christensen (2001). All of these measured correlations reported in the literature are in very good qualitative agreement with figure 6. One metric of this similarity is the tilt angle of the contours. Christensen & Wu (2005) attempted to quantify the tilt angle of the iso-contours of the correlation magnitude by identifying the points on each iso-contour that are furthest from the reference location. The combination of points from several iso-contours were fitted with a line to determine average slope of the contours. The average slope plotted vs. y_{ref} is shown in figure 8. The mean value was found to be 11.0°, which is identical to the mean angle found by Christensen & Wu.

As an additional comparison to existing literature, it is interesting to compare the present results with those of Liu, Adrian & Hanratty (2001), which presents two-point correlations from PIV measurements of a channel flow. Although the symmetry of the channel changes the character of the correlations significantly for y^+_{ref} near the

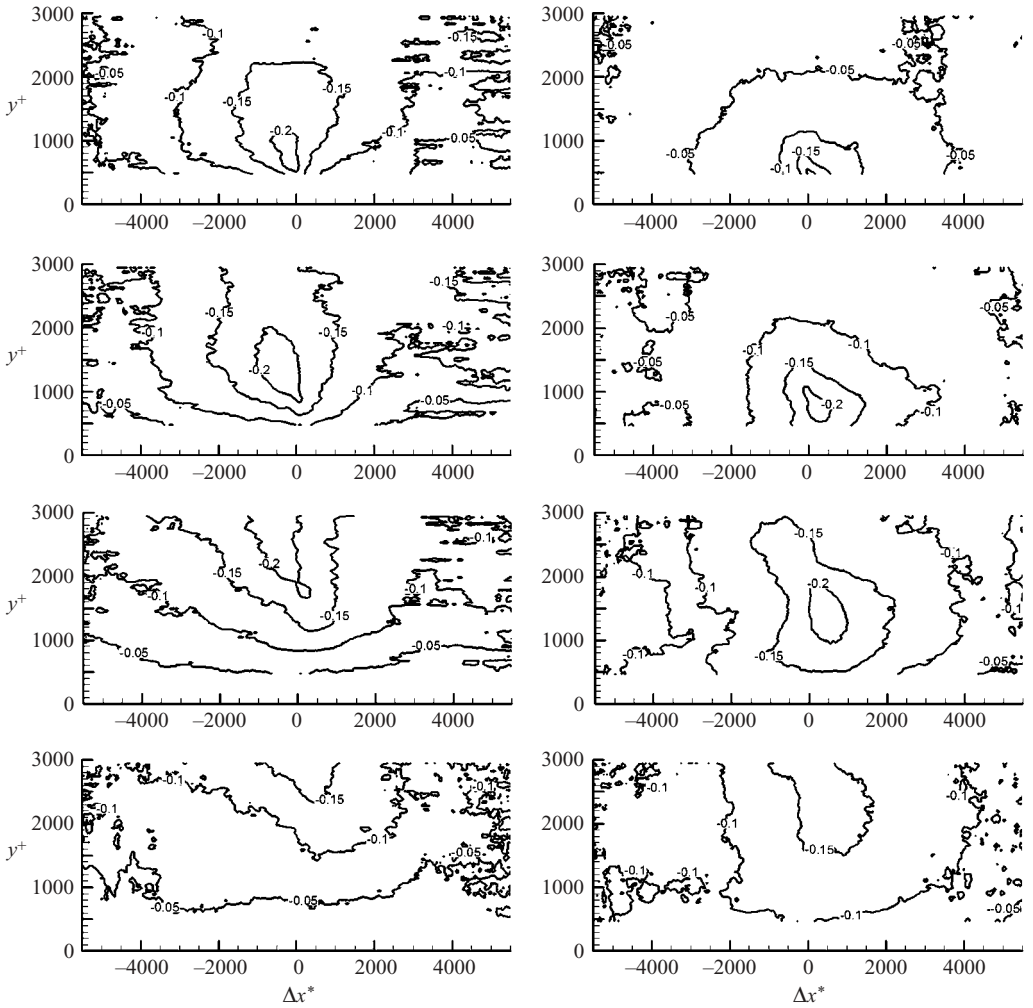

FIGURE 7. Two-point correlation functions R_{uv} (left) and R_{vu} (right). Fixed-point locations are the same as in figure 6.

centreline, it can be observed that the correlation contours for the wall-layer values of y^+_{ref} are in substantial qualitative agreement with figure 6.

The vertical velocity correlation, R_{vv}, is also shown in figure 6. These contours are quite distinctive from the streamwise velocity correlations in that the length scale, observed by the extent of the non-zero correlation values in both x and y directions, is limited. Also, the correlations are slightly elongated in the vertical direction. These features were also observed in the channel data of Liu *et al.* (2001).

The cross-correlation contours, R_{uv} and R_{vu} are shown in figure 7. These data are important because they provide information about the scales of motion that underlie the Reynolds stress $\overline{u'v'}$. The R_{uv} components show significant order in the structure, with a 'tilt' in the contour values towards the upstream direction, and significant correlation values over a large streamwise extent. The R_{vu} contours show similar features.

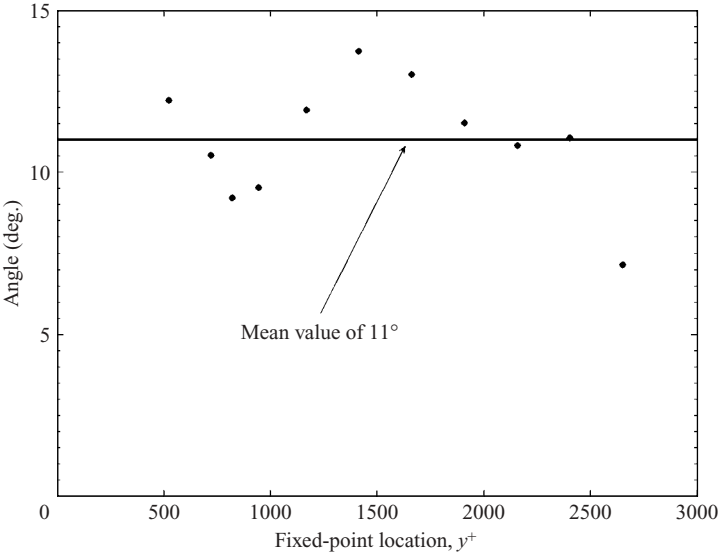

FIGURE 8. Average inclination angle of R_{uu} contours.

The qualitative consistency of the two-point correlations with those published previously suggests that the flow structure leading to these correlations is similar for a very wide range of Reynolds numbers. Liu *et al.* (2001) as well as Ganapathisubramani *et al.* (2005) conjecture that these contours are consistent with recent models of the near-wall coherent motions. The exact scaling of the contours is, however, not yet clear. Formally, the streamwise extent of any specified correlation value, say ΔX_R, will be a function of y_{ref}, ν/u_τ, and δ. The dimensionless functional form can therefore be written as $\Delta X_R^+ = \text{func}\,(y_{ref}^+, \delta^+)$ or $\Delta X_R/\delta = \text{func}\,(y_{ref}/\delta, \delta^+)$. Although the formal choice of scaling is arbitrary, it is intuitive that inner scaling (ΔX_R^+) seems appropriate for small y_{ref} values, and $\Delta X_R/\delta$ is more appropriate for y_{ref} farther from the surface. Naturally, what qualifies large or small y_{ref} magnitude depends on the Reynolds number, δ^+, of the experiment.

4. Characterization of near-surface structure

The instantaneous structure of the turbulent motions in the log and outer layers has also been studied extensively. A predominant feature observed in the instantaneous realizations is localized shear regions that are inclined at shallow angles to the wall. These regions of shear were documented in flow visualization by, for example, Head & Bandyopadhyay (1979) and Utami & Ueno (1987). Space–time correlation techniques using hot wires and hot films have also been interpreted to confirm the existence of these shear layers (see e.g. Johansson, Alfredsson & Eckelmann (1987), and Labraga *et al.* (2002)). Adrian, Meinhart & Tomkins (2000) obtained PIV realizations over almost the entire extent of the boundary layer thickness, and found evidence of inclined shear regions in 80 % percent of their realizations.

A corollary to the idea of inclined shear layers is the existence of uniform-momentum regions within the boundary layer. These are regions of fluid that lie between the thin shear layers that exhibit little net shear. The existence and statistical description of these regions of constant momentum is described by Meinhart & Adrian

(1995) and Adrian *et al.* (2000). Specifically, histogram plots of the streamwise velocity from individual PIV realizations typically indicated two, or sometimes three, local maxima. This supports the visual observation that distinct regions exist within the flow that have approximately constant streamwise velocity.

The inclined shear layers have been observed to be composed of discrete vortex-like motions in a number of laboratory studies. Bandyopadhyay (1980) and Head & Bandyopadhyay (1981) presented flow visualization evidence of hairpin-like vortices populating turbulent boundary layers. More recently, Adrian *et al.* (2000), Christensen & Adrian (2001), Tomkins & Adrian (2002), and Ganapathisubramani, Longmire & Marusic (2003) have all presented PIV results that support the notion that hairpin-like vortices organize into spatially distributed packets. Hutchins, Hambleton & Marusic (2005) have recently used PIV with various laser sheet orientations to better determine the three-dimensional character of the turbulent structure. They found substantial evidence supporting the concept of extensive low-momentum zones bounded by narrow regions containing discrete vortex-like motions.

One of the original motivations of the present research was to investigate the extent to which the vortex packet paradigm applies to very high-Reynolds-number flows. This issue was first addressed at the SLTEST sight by Hommema & Adrian (2003). In that study, flow visualization images were used to observe the nature of the flow structure using a smoke flair that was buried under the surface. They observed that the seeded fluid from the wall formed 'ramps' of various sizes that closely resembled the vortex packet structures observed in laboratory flows. These ramps were a predominant feature of the flow, and most flow visualization images contained multiple examples of ramp-like structures at various length scales.

Although large-scale visualization was not the primary focus of the present work, it can be stated anecdotally that the observations that are well-documented in Hommema & Adrian (2003) were commonly observed throughout the current measurements as well. For example, a short-duration release of seeding fluid (that often occurred during the set-up and calibration phases of an experiment) would reveal a region of fluid that would travel in the streamwise direction near the surface for some distance, and then suddenly lift away from the ground to form a ramp-like shape that was of order 30° from the surface. These features were observed during highly unstable conditions during daylight hours, as well as during highly stable conditions after sunset.

Initial visual inspection of the velocity vector maps provided a clear indication that all of the images could be represented as being in one of two general categories. The first group of images indicates little or no coherent structure, with a nearly uniform streamwise velocity over the measurement domain. Approximately 60 % of the acquired realizations were found to be in this category. An example realization is shown in figure 9. This finding is thought to be consistent with the concept of uniform-momentum zones described by Meinhart & Adrian (1995). That is, the occurrence of a momentum zone that is larger than the PIV field of view would result in observations similar to figure 9.

The second category of realizations can be described as having two regions of relatively constant streamwise velocity, separated by a thin sheared region. This group represented the remaining 40 % of the images. Moreover, the vast majority of the shear layers were found to be inclined at an angle to the wall. Figures 10 and 11 represent typical realizations within this group. In both realizations the vectors and velocity contours clearly indicate higher-momentum fluid occupying the upper left portion of the image, with lower-momentum fluid in the lower right.

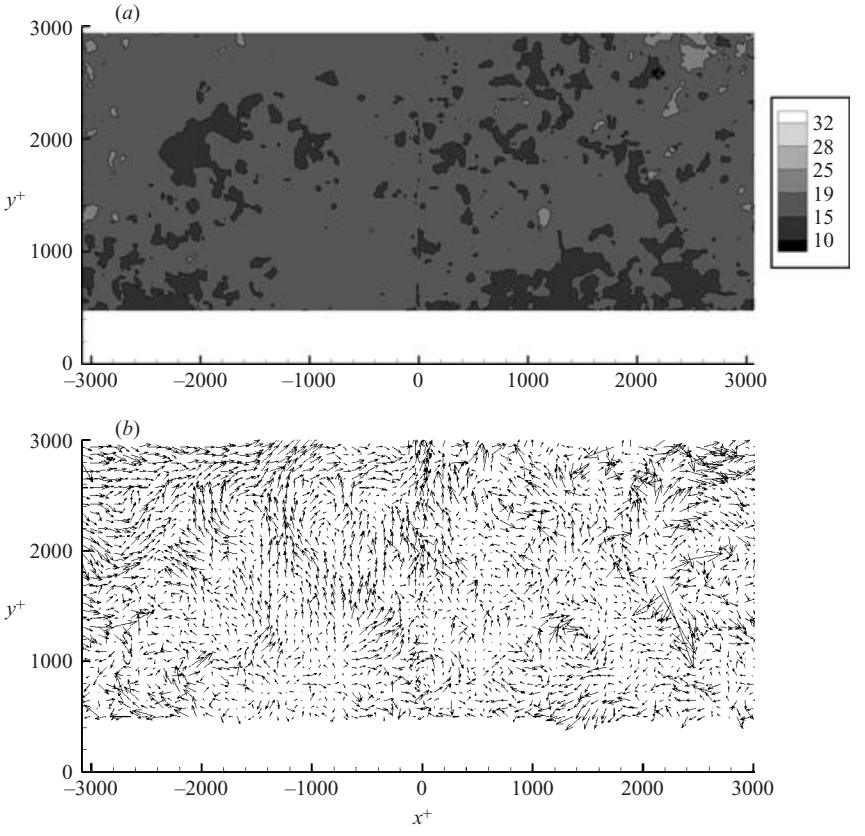

FIGURE 9. Single PIV realization indicating relatively low net shear. (*a*) Contours of u^+ magnitude, and (*b*) a vector map with $1.5\,\mathrm{m\,s^{-1}}$ subtracted from the u velocity.

As noted earlier, Adrian *et al.* (2000) were able to identify the existence of multiple momentum zones within a single PIV realization by computing the histogram of $u(x, y)$ for the entire field of view. The existence of multiple peaks in this histogram was then interpreted as a quantitative measure of multiple momentum zones. The histograms computed for the realizations of figures 10 and 11 are shown in figure 12. Like those computed by Adrian *et al.* (2000), these data distinctly show two peaks in the histogram, indicating that indeed there are two nominally uniform momentum zones within the field of view.

The angle of the sheared region that separated the regions of uniform velocity has been of some interest. For the present work, this angle was identified simply by inspecting the images one at a time. Specifically, an undergraduate student without any preconceived notions regarding near-wall shear layers was asked to look for unambiguous cases of shear layers from the velocity contours and mark a line segment parallel to the contours. The angle was determined for each of the 708 realizations for which a distinct region of shear could be identified. The mean value of the angle was found to be 14.9°, which is in substantial agreement with previous measurements at low Reynolds number. For example, Labraga *et al.* (2002) found a mean shear layer angle of 15.5° for $y^+ > 30$. Furthermore, Labraga *et al.* compiled results from 10 previous studies that document the existence of thin shear regions in

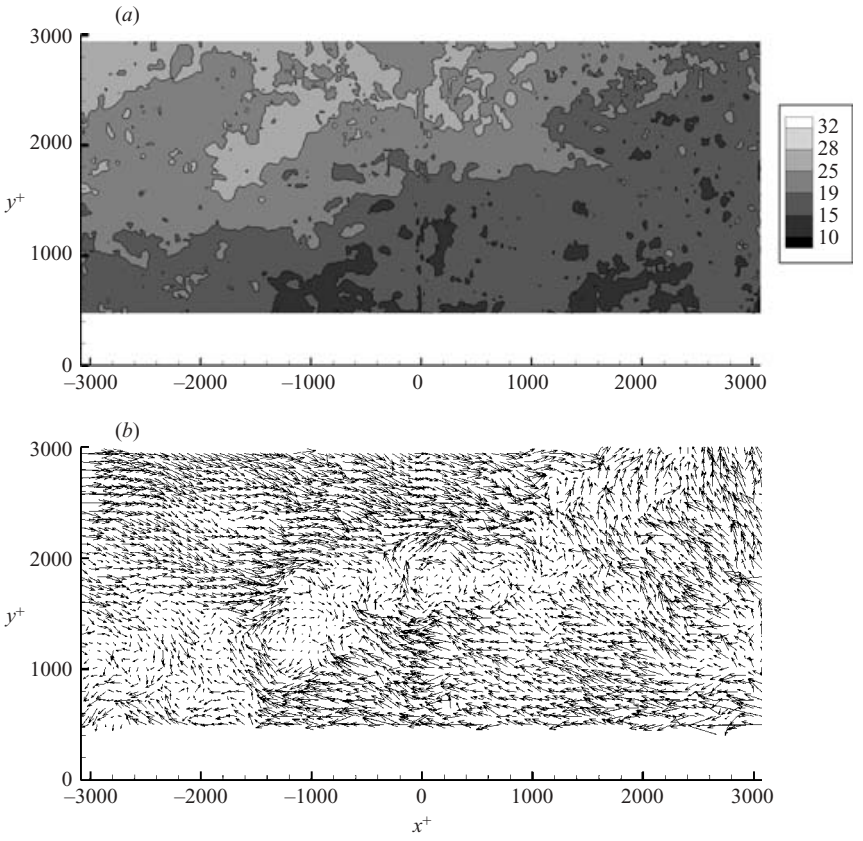

FIGURE 10. Single PIV realization indicating the presence of an inclined region of shear. (*a*) Contours of u magnitude, and (*b*) a vector map with $1.8\,\mathrm{m\,s^{-1}}$ subtracted from the u velocity.

the buffer region of the boundary layer. These studies typically found a mean angle of 15°, with approximately $\pm 3°$ of variability depending on the study. The Reynolds number based on momentum thickness, Re_θ was typically of the order 6000, with a maximum of $Re_\theta = 17\,500$ obtained by Head & Bandyopadhyay (1981).

It is interesting to note that measurements of the shear-layer angle obtained by processing flow visualization images typically results in slightly higher values. For example, Klewicki & Hirschi (2004), Head & Bandyopadhyay (1981) and Utami & Ueno (1987) each used flow visualization at low Reynolds number to obtain a mean shear layer angle of 29°, 20°, and 19°, respectively. Hommema & Adrian (2003) found a mean angle of 18.7° based on their visualization experiments at the SLTEST site.

Although the general paradigm of the uniform-momentum zones and inclined shear layers is strongly supported by the present measurements, the existence of coherent vortex motions, or packets, was not found to be a common feature. The realizations shown in figures 10 and 11 are good examples. Specifically, the regions of high shear were not found to be populated with smaller regions of compact rotation as was found in, for example, the PIV results of Christensen & Adrian (2001). Conditional averages of the flow field based on local swirl strength (and other metrics of vortices)

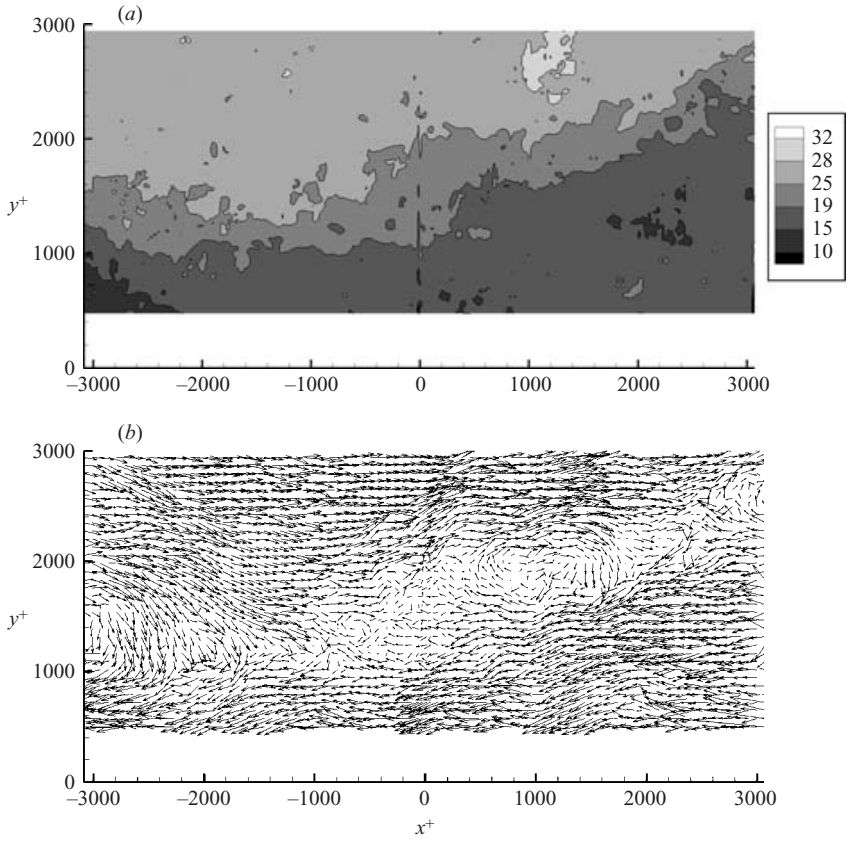

FIGURE 11. A second PIV realization indicating the presence of an inclined region of shear. (*a*) Contours of u magnitude, and (*b*) a vector map with $2.0\,\mathrm{m\,s^{-1}}$ subtracted from the u velocity.

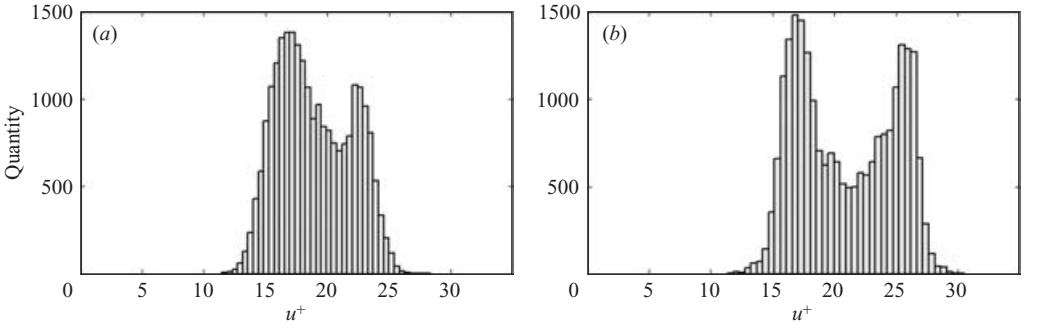

FIGURE 12. Probability distributions of u^+ velocity for the realizations represented in (*a*) figures 10 and (*b*) 11, respectively.

were found to produce no general structure beyond the immediate region of the condition location, and the remainder of the field was found to be identical to the unconditional mean vector field.

A possible explanation of the existence of the inclined shear layers without clear signs of coherent hairpin vortex motions can be given based on what is understood

about the Reynolds number dependence of the coherent motions in *free* shear layers. Specifically, the existence of coherent motions in free shear flows at low Reynolds number is clear from linear theory, flow visualization, and experiment (Ho & Huerre 1984). At high Reynolds number, the existence of such structure has been verified qualitatively by the flow visualization results of, for example, Brown & Roshko (1974) and two-point correlation measurements of Pui & Gartshore (1979). However, instantaneous realizations of the velocity and vorticity fields of shear layers often do not exhibit obvious coherent features. For example, Oakley, Loth & Adrian (1996) obtained PIV measurements in a high-Reynolds-number two-stream shear layer. Their measurements indicated a very complex fine-scale structure in both the velocity and vorticity fields, with little or no evidence of the large-scale structures that are known to exist in two-stream shear layers. The implication of this argument for turbulent boundary layers is that hairpin-like structures could exist at very high Reynolds number, but these coherent motions may be difficult to identify due the significant small-scale motions that coexist with the larger, organized motions.

5. Conclusions

The objective of this research was to use PIV measurements to provide information regarding the nature of turbulent fluid motions and their statistics in a very high-Reynolds-number boundary layer. The SLTEST site provided nearly ideal conditions for this purpose. It is important to keep in mind when considering the results and conclusions of this study that the measurement region was different from laboratory studies. Specifically, the top of the PIV domain was located at $y/\delta \approx 0.005$, and $y^+ \approx 3100$.

The following are the main conclusions that have been drawn from the acquired data set.

1. A layer of approximately constant Reynolds stress was found to exist over a significant wall normal extent. Agreement to within 5 % was found between the PIV data and three nearby sonic anemometers located at surface-normal distances of up to 3.9 m.

2. The von Kármán constant was found to be $\kappa = 0.410$ based on friction velocity measurements derived from the mean Reynolds stress. Although the present measurements cannot be used as a measurement of the true value of κ under canonical conditions, the consistency of this result adds confidence that the present boundary conditions are a reasonable representation of a flat-plate boundary layer without significant pressure gradient or thermal stability effects.

3. The RMS values of both streamwise and wall-normal velocity were found to be roughly constant over the measurement domain. The magnitude of the streamwise intensities was consistent with previous SLTEST site results and were predicted by the model of Marusic *et al.* (1997).

4. The two-point correlations (R_{uu}, R_{vv}, R_{uv}, and R_{vu}) are qualitatively the same as has been measured in the logarithmic region of lower-Reynolds-number laboratory flows. For example, the elliptical shape and inclination of the contours of constant correlation is in strong agreement with lower-Reynolds-number results. The average 'tilt' angle of the R_{uu} contours was calculated and found to be 11.0 °, which is exactly the value found at lower Reynolds number (Christensen & Wu 2005).

5. The hypothesis put forth by Meinhart & Adrian (1995) regarding the existence of nearly uniform-momentum zones was strongly supported by the present observations. Specifically, 60 % of the vector realizations were found to indicate almost no net

shear. This suggests that the entire field of view was enclosed within a larger zone of roughly uniform momentum. Two zones of approximately uniform momentum were found to be separated by inclined regions of shear in the remaining 40 % of the images.

6. The existence of uniform-momentum regions, inclined shear layers, and the similarity of the two-point correlations with lower-Reynolds-number measurements indicate that many of the statistical and instantaneous features found at low Reynolds number are also represented in the high-Reynolds-number flow. The present results also indicate a diminished organization of the turbulent motions within the regions of shear when compared to lower-Reynolds-number studies. Furthermore, no large-scale spatial coherence was observed in conditionally averaged calculations. These features are interpreted to be a result of the increased small-scale turbulent activity that is present at high Reynolds number.

The authors would like to thank the National Science Foundation (Dr. Michael Plesniak) and the Office of Naval Research (Dr. Ronald Joslin) for their support of the SLTEST facility. Thanks also to Dr. Callum Gray of LaVision Inc. for providing the design of the data acquisition cart, and to Professor Eric Pardyjak for his thoughtful discussions on the effects of stratification in boundary layers.

REFERENCES

Adrian, R. J., Meinhart, C. D. & Tomkins, C. D. 2000 Vortex organization in the outer region of the turbulent boundary layer. *J. Fluid Mech.* **422**, 1–54.

Bandyopadhyay, P. 1980 Large structure with a characteristic upstream interface in turbulent boundary layers. *Phys. Fluids* **23**, 2326–2327.

Brown, G. L. & Roshko, A. 1974 On density effects and large structure in turbulent mixing layers. *J. Fluid Mech.* **64**, 775–816.

Christensen, K. T. 2001 Experimental investigation of acceleration and velocity fields in turbulent channel flow, PhD thesis, Department of Theoretical and Applied Mechanics, University of Illinois at Urbana-Champaign.

Christensen, K. T. & Adrian, R. J. 2001 Statistical evidence of hairpin vortex packets in wall turbulence. *J. Fluid Mech.* **431**, 433–443.

Christensen, K. T. & Wu, U. 2005 Characteristics of vortex organization in the outer layer of wall turbulence. *Proc. Turbulent Shear Flows Phenomena 4, Blacksburg* VA. p. 1025.

DeGraaff, D. B. & Eaton, J. K. 2000 Reynolds-number scaling of the flat-plate turbulent boundary layer. *J. Fluid Mech.* **422**, 319–346.

Fernholz, H. H., Krause, E., Nockemann, M. & Shober, M. 1995 Comparative measurements in the canonical boundary layer at $Re < 6 \times 10^4$ on the wall of the German-Dutch wind tunnel. *Phys. Fluids.* **7**, 1275–1281.

Gad-el-Hak, M. & Bandyopadhyay, P. R. 1994 Reynolds number effects in wall-bounded turbulent flows. *Appl. Mech. Rev.* **47**, 307.

Ganapathisubramani, B., Hutchins, N., Hambleton, W. T., Longmire, E. K. & Marusic, I. 2005 Investigation of large-scale coherence in a turbulent boundary layer using two-point correlations. *J. Fluid Mech.* **524**, 57–80.

Ganapathisubramani, B., Longmire, E. K. & Marusic, I. 2003 Characteristics of vortex packets in turbulent boundary layers. *J. Fluid Mech.* **478**, 35–46.

Head, M. R. & Bandyopadhyay, P. 1981 New aspects of turbulent boundary-layer structure. *J. Fluid Mech.* **107**, 297–338.

Ho, C. & Huerre, P. 1984 Perturbed shear layers. *Annu. Rev. Fluid Mech.* **16**, 365–424.

Hommema, S. E. & Adrian, R. J. 2003 Packet structure of surface eddies in the atmospheric boundary layer. *Boundary-Layer Met.* **106**, 147–170.

Hutchins, N., Hambleton, W. T. & Marusic, I. 2005 Inclined cross-stream stereo particle image velocimetry measurements in turbulent boundary layers. *J. Fluid Mech.* **541**, 21–54.

Hutchins, N. & Marusic, I. 2006 Investigation of the log region structure in wall bounded turbulence. *AIAA Paper* 2006-0325.

Jimenez, J. 2004 Turbulent flows over rough walls. *Annu. Rev. Fluid Mech.* **36**, 173–196.

Johansson, A. V., Alfredsson, P. H. & Eckelmann, H. 1987 On the evolution of shear-layer structures in near-wall turbulence. In *Advances in Turbulence* (ed G. Comte-Bellot & J. Mathieu). Springer.

Kaimal, J. C. & Finnigan, J. J. 1994 *Atmospheric Boundary Layer Flows: Their Structure and Measurement*, Oxford University Press.

Klewicki, J. C. & Hirschi, C. R. 2004 Flow field properties local to near-wall shear layers in a low Reynolds number turbulent boundary layer. *Phys. Fluids* **16**, 4163.

Klewicki, J. C., Metzger, M. M., Kelner, E. & Thurlow, E. M. 1995 Viscous sublayer flow visualizations at $r_\theta = 1,500,000$. *Phys. Fluids* **7**, 857.

Kovasznay, L., Kibens, V. & Blackwelder, R. 1970 Large-scale motion in the intermittent region of a turbulent boundary layer. *J. Fluid Mech.* **41**, 283–325.

Kunkel, G. J. & Marusic, I. 2006 Study of the near-wall-turbulent region of the high-Reynolds-number boundary layer using an atmospheric flow. *J. Fluid Mech.* **548**, 375–402.

Labraga, L., Lagraa, B., Mazouz, A. & Keirsbulck, L. 2002 Propagation of shear-layer structures in the near-wall region of a turbulent boundary layer. *Exps. Fluids* **33**, 670–676.

Liu, Z., Adrian, R. J. & Hanratty, T. J. 2001 Large-scale modes of turbulent channel flow: transport and structure. *J. Fluid Mech.* **448**, 53–80.

Marusic, I. & Kunkel, G. J. 2003 Streamwise turbulence intensity formulation for flat-plate boundary layers. *Phys. Fluids* **15**, 2461.

Marusic, I., Uddin, A. K. M. & Perry, A. E. 1997 Similarity law for the streamwise turbulence intensity in zero-pressure-gradient turbulent boundary layers. *Phys. Fluids* **9**, 3718.

McKeon, B. J., Li, J., Jiang, W., Morrison, J. & Smits, A. 2004 Further observations on the mean velocity distribution in fully developed pipe flow. *J. Fluid Mech.* **501**, 135–147.

McNaughton, K. G., Clement, R. & Moncrieff, J. B. 2006 Turbulence spectra above the surface friction layer in a convective boundary layer. *Proc. 17th Symp. on Boundary Layers and Turbulence, American Meteorological Society, San Diego, CA, May 2006, paper* 1.3.

Meinhart, C. D. & Adrian, R. J. 1995 On the existence of uniform momentum zones in a turbulent boundary layer. *Phys. Fluids* **7**, 694.

Metzger, M. & Klewicki, J. 2001 A comparative study of near-wall turbulence in high and low Reynolds number boundary layers. *Phys. Fluids* **13**, 692–701.

Metzger, M., Klewicki, J., Bradshaw, K. & Sadr, R. 2001 Scaling the near-wall axial turbulent stress in the zero pressure gradient boundary layer. *Phys. Fluids.* **13**, 1819–1821.

Morris, S. C. & Foss, J. F. 2003 The non-self similar scaling of vorticity in a shear layer. *Proc. IUTAM Symp. on Reynolds Number Scaling in Turbulent Flow*. (ed. A. J. Smiths). Kluwer.

Morris, S. C. & Foss, J. F. 2005 Vorticity spectra in high Reynolds number anisotropic turbulence. *Phys. Fluids.* **17**, 088102.

Oakley, T. R., Loth, E. & Adrian, R. J. 1996 Cinematic particle image velocimetry of high-Reynolds-number turbulent free shear layer. *AIAA J.* **34**, 299.

Panofsky, H. & Dutton, J. 1983 *Atmospheric Turbulence: Models and Methods for Engineering Applications.* Wiley-Interscience.

Priyadarshana, P. J. A. & Klewicki, J. C. 2004 Study of the motions contributing to the Reynolds stress in high and low Reynolds number turbulent boundary layers. *Phys. Fluids.* **16**, 4586–4600.

Pui, N. K. & Gartshore, I. S. 1979 Measurements of the growth rate and structure in plane turbulent mixing layers. *J. Fluid Mech.* **91**, 111–130.

Sreenivasan, K. R. 1989 The turbulent boundary layer. In *Frontiers in Experimental Fluid Mechanics* (ed. M. Gad-el-Hak), pp 159–209, Lecture Notes in Engineering, Vol. 46, Springer.

Stolpa, S. 2004 Spatially resolved near surface motions in the atmospheric boundary layer. MS Thesis, Aerospace and Mechanical Engineering, University of Notre Dame.

Stull, R. B. 1988 *An Introduction to Boundary Layer Meteorology*, p. 377 Kluwer.

Tomkins, C. D. & Adrian, R. J. 2003 Spanwise structure and scale growth in turbulent boundary layers. *J. Fluid Mech.* **490**, 37–74.

Utami, T. & Ueno, T. 1987 Experimental study on the coherent structure of turbulent open channel flow using visualization and picture processing. *J. Fluid Mech.* **174**, 399–440.